Supplemental information of "many-body critical non-Hermitian skin effect"

Yi Qin,[1] Yee Sin Ang,[1] Ching Hua Lee,[2,*] and Linhu Li[3,†]

[1] *Science, Mathematics and Technology, Singapore University of Technology and Design, Singapore 487372, Singapore*
[2] *Department of Physics, National University of Singapore, Singapore 117542*
[3] *Quantum Science Center of Guangdong-Hong Kong-Macao Greater Bay Area (Guangdong), Shenzhen, China*

Supplemental Note 1. PERTURBATION TREATMENT FOR THE BOUND CLUSTER STATES

In this section, we derive the effective model for the bound states critical skin effect. The model Hamiltonian can be written as [S1, S2]

$$\begin{aligned}\hat{H} = &-\sum_{j=1,\sigma=A,B}^{L-1}\left[J_L^{\sigma}\hat{a}_{j,\sigma}^{\dagger}\hat{a}_{j+1,\sigma}+J_R^{\sigma}\hat{a}_{j+1,\sigma}^{\dagger}\hat{a}_{j,\sigma}\right]\\&+J_p\sum_{j=1}^{L}\left(\hat{a}_{j,A}^{\dagger}\hat{a}_{j,B}+\hat{a}_{j,B}^{\dagger}\hat{a}_{j,A}\right)\\&+\frac{U}{2}\sum_{j=1,\sigma=A,B}^{L}\hat{n}_{j,\sigma}(\hat{n}_{j,\sigma}-1)\\&+\mu\sum_{j=1}^{L}\left(\hat{n}_{j,A}-\hat{n}_{j,B}\right).\end{aligned}\tag{S1}$$

In the paired subspace, we take the unperturbed term as

$$\hat{H}_0=\frac{U}{2}\sum_{j=1,\sigma=A,B}^{L}\hat{n}_{j,\sigma}(\hat{n}_{j,\sigma}-1)+\mu\sum_{j=1}^{L}\left(\hat{n}_{j,A}-\hat{n}_{j,B}\right).\tag{S2}$$

The perturbation term is given by

$$\begin{aligned}\hat{H}_{\text{hop}} = &-\sum_{j=1,\sigma=A,B}^{L-1}\left[J_L^{\sigma}\hat{a}_{j,\sigma}^{\dagger}\hat{a}_{j+1,\sigma}+J_R^{\sigma}\hat{a}_{j+1,\sigma}^{\dagger}\hat{a}_{j,\sigma}\right]\\&+J_p\sum_{j=1}^{L}\left(\hat{a}_{j,A}^{\dagger}\hat{a}_{j,B}+\hat{a}_{j,B}^{\dagger}\hat{a}_{j,A}\right).\end{aligned}\tag{S3}$$

Then, we project the Hamiltonian into the paired subspace $|a_{l,\sigma}^2\rangle=\frac{1}{\sqrt{2}}\left(\hat{a}^{\dagger}\right)_{l,\sigma}^2|\text{vac}\rangle\equiv|\,\beta_{l,\sigma}\rangle\rangle,(l=1,2,...,L;\sigma=A,B)$, with $|\text{vac}\rangle$ the vacuum state. This basis constitutes a sub-Hilbert space of the Fock space, whose basis can be denoted as $|l_1\sigma_1,l_2\sigma_2\rangle,1\leq l_1\leq l_2\leq L,\sigma_{1,2}=A,B.$, with L the number of unit cell), and (l_1,l_2) the positions of the bosons.

$$\hat{H}_{\text{eff}}\ =E_0+\hat{P}_{\text{int}}\,\hat{H}_{\text{hop}}\,\hat{P}_{\text{int}}\ +\hat{P}_{\text{int}}\,\hat{H}_{\text{hop}}\,\left(E_0-\hat{H}_{\text{int}}\right)^{-1}\hat{H}_{\text{hop}}\,\hat{P}_{\text{int}}\ +O\left(\hat{H}_{\text{hop}}^3\right),\tag{S4}$$

$\hat{P}_{\text{int}}=\sum_{l=1,\sigma=A,B}^{L}|\beta_{l,\sigma}\rangle\rangle\,\langle\langle\beta_{l,\sigma}|$ the projector onto the doubly occupied sub-Hilbert space and $E=U-2\delta_{\sigma,A}\mu+2\delta_{\sigma,B}\mu$. The firstorder perturbation $\widehat{P}_{\text{int}}\,\hat{H}_{\text{hop}}\,\hat{P}_{\text{int}}$ is zero.

* phylch@nus.edu.sg
† lilinhu@quantumsc.cn

$$
\begin{aligned}
&\langle\langle \beta_{j,\sigma}|\, \hat{H}_{\rm hop} \left(E_0 - \hat{H}_0\right)^{-1} \hat{H}_{\rm hop} \mid \beta_{i,\sigma}\rangle\rangle \\
&= \frac{1}{2}\langle {\rm vac}|\hat{a}^2_{j,\sigma} \hat{H}_{\rm hop} \left(E_0 - \hat{H}_0\right)^{-1} \hat{H}_{\rm hop} \left(\hat{a}^\dagger_{i,\sigma}\right)^2 |{\rm vac}\rangle. \\
&\Bigg[- \sum_{l=1}^{L-1} \left(J^A_L \hat{a}^\dagger_{l,A} \hat{a}_{l+1,A} + J^A_R \hat{a}^\dagger_{l+1,A} \hat{a}_{l,A} \right) - \sum_{l=1}^{L-1} \left(J^B_L \hat{a}^\dagger_{l,B} \hat{a}_{l+1,B} + J^B_R \hat{a}^\dagger_{l+1,B} \hat{a}_{l,B} \right) \\
&+ J_p \sum_{l=1}^{L} \left(\hat{a}^\dagger_{l,A} \hat{a}_{l,B} + \hat{a}^\dagger_{l,B} \hat{a}_{l,A} \right) \Bigg] \frac{\left(\hat{a}^\dagger_{i,\sigma}\right)^2}{\sqrt{2}} |{\rm vac}\rangle \\
&= -\delta_{\sigma,A} \left(J^A_L \hat{a}^\dagger_{i-1,A} \hat{a}^\dagger_{i,A} + J^A_R \hat{a}^\dagger_{i+1,A} \hat{a}^\dagger_{i,A} \right) |{\rm vac}\rangle \\
&- \delta_{\sigma,B} \left(J^B_L \hat{a}^\dagger_{i-1,B} \hat{a}^\dagger_{i,B} + J^B_R \hat{a}^\dagger_{i+1,B} \hat{a}^\dagger_{i,B} \right) |{\rm vac}\rangle \\
&+ \delta_{\sigma,A} J_p \hat{a}^\dagger_{i,B} \hat{a}_{i,A} |{\rm vac}\rangle + \delta_{\sigma,B} J_p \hat{a}^\dagger_{i,A} \hat{a}_{i,B} |{\rm vac}\rangle
\end{aligned}
$$

Thus, we can divide the calculations into four sectors.

$$
\begin{aligned}
&\left(E_0 - \hat{H}_0\right)^{-1} \hat{H}_{\rm hop} \left(\hat{a}^\dagger_{i,\sigma}\right)^2 |{\rm vac}\rangle \\
&= -\delta_{A,\sigma} \left(E_0 - \hat{H}_0\right)^{-1} \left(J^A_L \hat{a}^\dagger_{i-1,A} \hat{a}^\dagger_{i,A} + J^A_R \hat{a}^\dagger_{i+1,A} \hat{a}^\dagger_{i,A} \right) |{\rm vac}\rangle \\
&- \delta_{B,\sigma} \left(E_0 - \hat{H}_0\right)^{-1} \left(J^B_L \hat{a}^\dagger_{i-1,B} \hat{a}^\dagger_{i,B} + J^B_R \hat{a}^\dagger_{i+1,B} \hat{a}^\dagger_{i,B} \right) |{\rm vac}\rangle \\
&+ \delta_{A,\sigma} \left(E_0 - \hat{H}_0\right)^{-1} J_p \hat{a}^\dagger_{i,B} \hat{a}_{i,A} |{\rm vac}\rangle \\
&+ \delta_{B,\sigma} \left(E_0 - \hat{H}_0\right)^{-1} J_p \hat{a}^\dagger_{i,A} \hat{a}_{i,B} |{\rm vac}\rangle \\
&= -\delta_{A,\sigma} \frac{1}{U + 2\mu - 2\mu} \left(J^A_L \hat{a}^\dagger_{i-1,A} \hat{a}^\dagger_{i,A} + J^A_R \hat{a}^\dagger_{i+1,A} \hat{a}^\dagger_{i,A} \right) |{\rm vac}\rangle \\
&- \delta_{B,\sigma} \frac{1}{U - 2\mu - (-2\mu)} \left(J^B_L \hat{a}^\dagger_{i-1,B} \hat{a}^\dagger_{i,B} + J^B_R \hat{a}^\dagger_{i+1,B} \hat{a}^\dagger_{i,B} \right) |{\rm vac}\rangle \\
&+ \delta_{A,\sigma} \frac{1}{U + 2\mu} J_p \hat{a}^\dagger_{i,B} \hat{a}_{i,A} |{\rm vac}\rangle \\
&+ \delta_{B,\sigma} \frac{1}{U - 2\mu} J_p \hat{a}^\dagger_{i,A} \hat{a}_{i,B} |{\rm vac}\rangle \\
&= -\delta_{A,\sigma} \frac{1}{U} \left(J^A_L \hat{a}^\dagger_{i-1,A} \hat{a}^\dagger_{i,A} + J^A_R \hat{a}^\dagger_{i+1,A} \hat{a}^\dagger_{i,A} \right) |{\rm vac}\rangle \\
&- \delta_{B,\sigma} \frac{1}{U} \left(J^B_L \hat{a}^\dagger_{i-1,B} \hat{a}^\dagger_{i,B} + J^B_R \hat{a}^\dagger_{i+1,B} \hat{a}^\dagger_{i,B} \right) |{\rm vac}\rangle \\
&+ \delta_{A,\sigma} \frac{1}{U + 2\mu} J_p \hat{a}^\dagger_{i,B} \hat{a}_{i,A} |{\rm vac}\rangle \\
&+ \delta_{B,\sigma} \frac{1}{U - 2\mu} J_p \hat{a}^\dagger_{i,A} \hat{a}_{i,B} |{\rm vac}\rangle
\end{aligned}
\tag{S5}
$$

Further derivation leads to

$$
\begin{aligned}
&\hat{H}_{\text{hopp}}\ \left(E_0-\hat{H}_0\right)^{-1}\hat{H}_{\text{bop}}\ \left(\hat{a}^\dagger_{i,\sigma}\right)^2|\text{vac}\rangle\\
&=\Bigg[-\sum_{i=1}^{L-1}\left(J_L^A\hat{a}^\dagger_{i-1,A}\hat{a}_{i,A}+J_R^A\hat{a}^\dagger_{i+1,A}\hat{a}_{i,A}\right)\\
&-\sum_{l=1}^{L-1}\left(J_L^B\hat{a}^\dagger_{i-1,B}\hat{a}_{i,B}+J_R^B\hat{a}^\dagger_{i+1,B}\hat{a}_{i,B}\right)\\
&+J_p\sum_{i=1}^{L}\left(\hat{a}^\dagger_{i,B}\hat{a}_{i,A}+\hat{a}^\dagger_{i,A}\hat{a}_{i,B}\right)\Bigg]\\
&\times\Bigg[-\delta_{\sigma,A}\frac{1}{U}\left(J_L^A\hat{a}^\dagger_{i-1,A}\hat{a}^\dagger_{i,A}+J_R^A\hat{a}^\dagger_{i+1,A}\hat{a}^\dagger_{i,A}\right)|\text{vac}\rangle\\
&-\delta_{\sigma,B}\frac{1}{U}\left(J_L^B\hat{a}^\dagger_{i-1,B}\hat{a}^\dagger_{i,B}+J_R^B\hat{a}^\dagger_{i+1,B}\hat{a}^\dagger_{i,B}\right)|\text{vac}\rangle\\
&+\delta_{\sigma,A}\frac{1}{U+2\mu}J_p\hat{a}^\dagger_{i,B}\hat{a}^\dagger_{i,A}|\text{vac}\rangle+\delta_{\sigma,B}\frac{1}{U-2\mu}J_p\hat{a}^\dagger_{i,A}\hat{a}^\dagger_{i,B}|\text{vac}\rangle\Bigg]\Bigg]
\end{aligned}
$$

$$
\begin{aligned}
&=\delta_{\sigma,A}\frac{1}{U}\Big[J_L^AJ_L^A\hat{a}^\dagger_{i-2,A}\hat{a}^\dagger_{i,A}+\sqrt{2}J_L^AJ_L^A\hat{a}^\dagger_{i-1,A}\hat{a}^\dagger_{i-1,A}\\
&+2J_L^AJ_R^A\hat{a}^\dagger_{i-1,A}\hat{a}^\dagger_{i+1,A}+2\sqrt{2}J_L^AJ_R^A\hat{a}^\dagger_{i,A}\hat{a}^\dagger_{i,A}+\sqrt{2}J_R^AJ_R^A\hat{a}^\dagger_{i+1,A}\hat{a}^\dagger_{i+1,A}\\
&+J_R^AJ_R^A\hat{a}^\dagger_{i+2,A}\hat{a}^\dagger_{i,A}\Big]|\text{vac}\rangle\\
&+\delta_{\sigma,B}\frac{1}{U}\Big[J_L^BJ_L^B\hat{a}^\dagger_{i-2,B}\hat{a}^\dagger_{i,B}+\sqrt{2}J_L^BJ_L^B\hat{a}^\dagger_{i-1,B}\hat{a}^\dagger_{i-1,B}\\
&+2J_L^BJ_R^B\hat{a}^\dagger_{i-1,B}\hat{a}^\dagger_{i+1,B}+2\sqrt{2}J_L^BJ_R^B\hat{a}^\dagger_{i,B}\hat{a}^\dagger_{i,B}+\sqrt{2}J_R^BJ_R^B\hat{a}^\dagger_{i+1,B}\hat{a}^\dagger_{i+1,B}\\
&+J_R^BJ_R^B\hat{a}^\dagger_{i+2,B}\hat{a}^\dagger_{i,B}\Big]|\text{vac}\rangle\\
&+\delta_{\sigma,A}\frac{\sqrt{2}}{U+2\mu}J_pJ_p\hat{a}^\dagger_{i,A}\hat{a}^\dagger_{i,A}|\text{vac}\rangle+\delta_{\sigma,B}\frac{\sqrt{2}}{U-2\mu}J_pJ_p\hat{a}^\dagger_{i,B}\hat{a}^\dagger_{i,B}|\text{vac}\rangle\\
&+\delta_{\sigma,A}\frac{\sqrt{2}}{U-2\mu}J_pJ_p\hat{a}^\dagger_{i,A}\hat{a}^\dagger_{i,A}|\text{vac}\rangle+\delta_{\sigma,B}\frac{\sqrt{2}}{U+2\mu}J_pJ_p\hat{a}^\dagger_{i,B}\hat{a}^\dagger_{i,B}|\text{vac}\rangle
\end{aligned}
$$

Finally, we obtain the results.

$$
\begin{aligned}
&\frac{1}{2}\langle\text{vac}\,|\hat{a}^2_{j,\sigma'}\hat{H}_{\text{hop}}\left(E_0-\hat{H}_0\right)^{-1}\hat{H}_{\text{hop}}\left(\hat{a}^\dagger_{i,\sigma}\right)^2|\text{vac}\rangle\\
&=\delta_{A,\sigma}\delta_{A,\sigma'}\frac{\sqrt{2}}{U}\left[J_L^AJ_L^A\delta_{j,i-1}+2J_L^AJ_R^A\delta_{j,i}+J_R^AJ_R^A\delta_{j,i+1}\right]\\
&+\delta_{B,\sigma}\delta_{B,\sigma'}\frac{\sqrt{2}}{U}\left[J_L^BJ_L^B\delta_{j,i-1}+2J_L^BJ_R^B\delta_{j,i}+J_R^BJ_R^B\delta_{j,i+1}\right]\\
&+\delta_{A,\sigma}\delta_{B,\sigma'}J_pJ_p\left[\frac{\sqrt{2}}{U+2\mu}\delta_{j,i}+\frac{\sqrt{2}}{U-2\mu}\delta_{j,i}\right]\\
&+\delta_{B,\sigma}\delta_{A,\sigma'}J_pJ_p\left[\frac{\sqrt{2}}{U-2\mu}\delta_{j,i}+\delta_{j,i}\frac{\sqrt{2}}{U+2\mu}\right]
\end{aligned}
\tag{S6}
$$

Thus, the effective Hamiltonian can be written as

$$\begin{aligned}
H_{\text{eff}} =& U + \sum_{l=1}^{L}\left[\left(\frac{\sqrt{2}J_p^2}{U} + \frac{2\sqrt{2}J_L^A J_R^A}{U}\right)|\beta_{l,A}\rangle\!\rangle\langle\!\langle\beta_{l,A}|\right] \\
&+ \sum_{l=1}^{L}\left[\left(\frac{\sqrt{2}J_p^2}{U} + \frac{2\sqrt{2}J_L^B J_R^B}{U}\right)|\beta_{l,B}\rangle\!\rangle\langle\!\langle\beta_{l,B}|\right] \\
&+ \frac{\sqrt{2}}{U}\sum_{l=1}^{L-1}\left[(J_L^A)^2|\beta_{l,A}\rangle\!\rangle\langle\!\langle\beta_{l+1,A}| + (J_R^A)^2|\beta_{l+1,A}\rangle\!\rangle\langle\!\langle\beta_{l,A}|\right] \\
&+ \frac{\sqrt{2}}{U}\sum_{l=1}^{L-1}\left[(J_L^B)^2|\beta_{l,B}\rangle\!\rangle\langle\!\langle\beta_{l+1,B}| + (J_R^B)^2|\beta_{l+1,B}\rangle\!\rangle\langle\!\langle\beta_{l,B}|\right] \\
&+ \sum_{l=1,\pm}^{L}\left[\frac{\sqrt{2}J_p^2}{U\pm+2\mu}|\beta_{l,B}\rangle\!\rangle\langle\!\langle\beta_{l,A}| + \frac{\sqrt{2}J_p^2}{U\pm 2\mu}|\beta_{l,A}\rangle\!\rangle\langle\!\langle\beta_{l,B}|\right].
\end{aligned} \tag{S7}$$

We find that the effective Hamiltonian of bound pair behaves like a single particle and the critical skin effect is naturally occurs. For simplicity, we will set $\mu = 0$ in the maintext and we have

$$\begin{aligned}
H_{\text{eff}} =& U + \sum_{l=1}^{L}\left[\left(\frac{\sqrt{2}J_p^2}{U} + \frac{2\sqrt{2}J_L^A J_R^A}{U}\right)|\beta_{l,A}\rangle\langle\beta_{l,A}|\right] \\
&+ \sum_{l=1}^{L}\left[\left(\frac{\sqrt{2}J_p^2}{U} + \frac{2\sqrt{2}J_L^B J_R^B}{U}\right)|\beta_{l,B}\rangle\langle\beta_{l,B}|\right] \\
&+ \frac{\sqrt{2}}{U}\sum_{l=1}^{L-1}\left[(J_L^A)^2|\beta_{l,A}\rangle\langle\beta_{l+1,A}| + (J_R^A)^2|\beta_{l+1,A}\rangle\langle\beta_{l,A}|\right] \\
&+ \frac{\sqrt{2}}{U}\sum_{l=1}^{L-1}\left[(J_L^B)^2|\beta_{l,B}\rangle\langle\beta_{l+1,B}| + (J_R^B)^2|\beta_{l+1,B}\rangle\langle\beta_{l,B}|\right] \\
&+ \frac{2\sqrt{2}J_p^2}{U}\sum_{l=1}^{L}\left[|\beta_{l,B}\rangle\langle\beta_{l,A}| + |\beta_{l,A}\rangle\langle\beta_{l,B}|\right].
\end{aligned} \tag{S8}$$

Note that in the main text we have $J_L^{A/B} = Je^{\pm\alpha}, J_R^{A/B} = Je^{\mp\alpha}$, thus the effective Hamiltonian written as

$$\begin{aligned}
H_{\text{eff}} =& U + \sum_{l=1}^{L}\left[\left(\frac{\sqrt{2}J_p^2}{U} + \frac{2\sqrt{2}J^2}{U}\right)|\beta_{l,A}\rangle\rangle\langle\langle\beta_{l,A}|\right] \\
&+ \sum_{l=1}^{L}\left[\left(\frac{\sqrt{2}J_p^2}{U} + \frac{2\sqrt{2}J^2}{U}\right)|\beta_{l,B}\rangle\rangle\langle\langle\beta_{l,B}|\right] \\
&+ \frac{\sqrt{2}J^2}{U}\sum_{l=1}^{L-1}\left[e^{2\alpha}|\beta_{l,A}\rangle\rangle\langle\langle\beta_{l+1,A}| + e^{-2\alpha}|\beta_{l+1,A}\rangle\rangle\langle\langle\beta_{l,A}|\right] \\
&+ \frac{\sqrt{2}J^2}{U}\sum_{l=1}^{L-1}\left[e^{-2\alpha}|\beta_{l,B}\rangle\rangle\langle\langle\beta_{l+1,B}| + e^{2\alpha}|\beta_{l+1,B}\rangle\rangle\langle\langle\beta_{l,B}|\right] \\
&+ \frac{2\sqrt{2}J_p^2}{U}\sum_{l=1}^{L}\left[|\beta_{l,B}\rangle\rangle\langle\langle\beta_{l,A}| + |\beta_{l,A}\rangle\rangle\langle\langle\beta_{l,B}|\right].
\end{aligned} \tag{S9}$$

Supplemental Note 2. THE CRITICAL BEHEAVIOUR FOR THE SCATTERING AND BOUND CLUSTER STATES

In the main text, we primarily present the results for a fixed chemical potential in both the scattering and bound CSE cases. However, the critical behavior can indeed be tuned by the onsite interaction U and the chemical potential μ, as shown in Supplemental Figure 1 (a) and (b). For the scattering cluster, max(ImE) remains unchanged with increasing interaction U but tends to become real as the chemical potential μ increases. In contrast, for the bound state cluster, max(ImE) decreases with increasing interaction strength U or chemical potential μ. In both cases, no CSE occurs if the chemical potential μ is sufficiently large to separate the overlapping clusters.

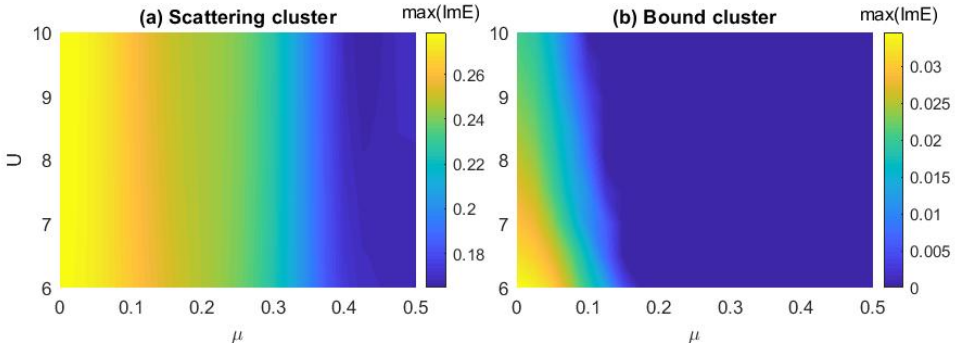

Supplemental Figure 1. The maximum imaginary energy states with different U and μ. (a) and (b) maximum imaginary energies for the scattering and bound cluster of $L = 15, J_p = 0.01$ respectively. Other parameters are the same as in the main text ($Je^{\alpha} = 1$ and $Je^{-\alpha} = 0.5$)..

Supplemental Note 3. DENSITY DISTRIBUTIONS IN REAL SPACE AND MORE EXAMPLES FOR MIXED CSE

To better highlighting our discovery, we have focused only on the joint cluster when discussing the mixed CSE in the main text. In this section, we provide the full information of density distributions and eigenenergies for each cluster at both $U = 16, \mu = 4$ and $U = 8, \mu = 4$ (the same parameters as in Fig. 3 in the main text), as shown in Fig. Supplemental Figure 2. The transitions that emerge with increasing system size can be clearly see from the density distribution for the LS-RB cluster [Supplemental Figure 2(a3) and (b3)], but not for the BiS-RB cluster Supplemental Figure 2(c2) and (d2)]. Additionally, we demonstrate the occurrence of a mixed CSE under negative interaction $U = -16, \mu = 4$, as shown in Supplemental Figure 3. In this case, the density distribution of the RS-LB cluster evolves from bipolar-localized to right-localized as the system size increases, indicating the emergence of a mixed CSE.

Then, we present a more intricate example of the mixed skin effect, involving the mixing of three scattering clusters, where one of the bound-state clusters is embedded within a scattering continuum. The corresponding energy spectrum and density distributions are shown in Supplemental Figure 4. The mixing between the bound-state cluster and the scattering cluster occurs when ReE approximatly falls between 2 and 3. The transition from real to complex eigenvalues is computed and illustrated in Supplemental Figure 4(d).

Supplemental Note 4. ENTROPY FOR THE MIXED CSE WITH $U = 16, \mu = 4$

In the main text, we have demonstrated the different density distributions at $L = 20$ and $L = 30$ for the joint cluster that exhibits mixed CSE. To further investigate the transition with increasing system size, we calculate the A-B chain entropy S_A and the left-right entropy S_{left} of the largest imaginary energy state of the joint LS-RB cluster ([see Supplemental Figure 2(a) and (b), and Fig. 3(b) in the main text] with the increasing the system size L, as shown in Supplemental Figure 5. These quantities are defined as [S3]

$$S_A = -\text{Tr}\rho_A \ln \rho_A \tag{S10}$$

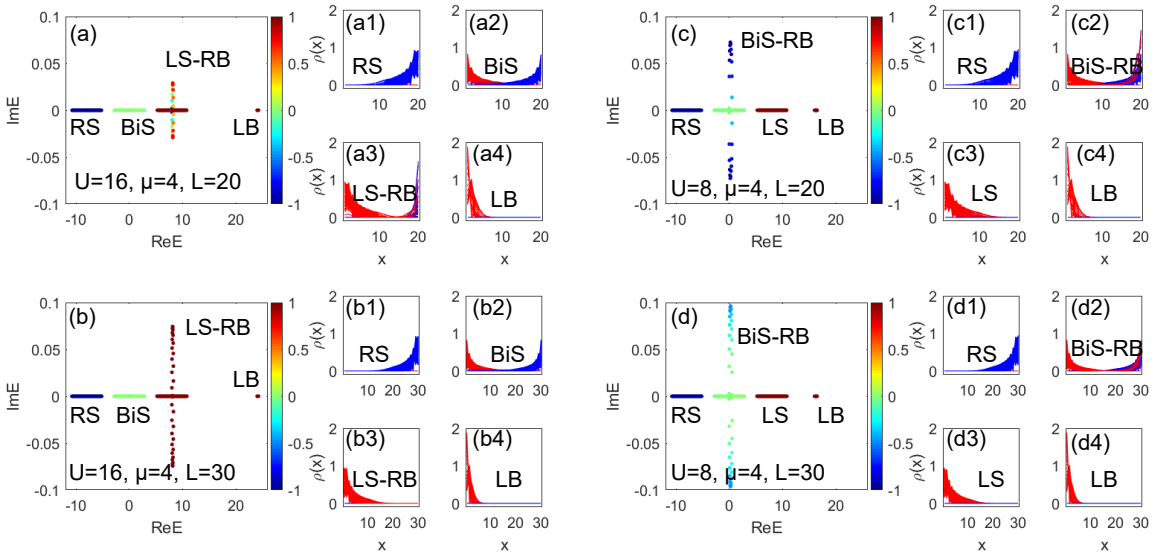

Supplemental Figure 2. The energy spectrum and density distributions versus system size L with $U = 16, \mu = 4$ and $U = 8, \mu = 4$ for $N = 2$. (a) The energy spectrum for $L = 20$ with $U = 16, \mu = 4$. (a1-a4) The densities of the energy clusters ordered by the real energy in (a) indicated by RS, BiS, LS-RB, and LB. (b) the same as (a) but for $L = 30$. (c) The energy spectrum for $L = 20$ with $U = 8, \mu = 4$. (c1-c4) The densities of the energy clusters ordered by the real energy in (c) indicated by RS, BiS-RB, LS, and LB. (d) the same as (c) but for $L = 30$. In all density plots, the red (blue) curve represents the density on the A (B) sublattice. $J_p = 0.01$ and other parameters are the same as in the main text ($Je^{\alpha} = 1$ and $Je^{-\alpha} = 0.5$).

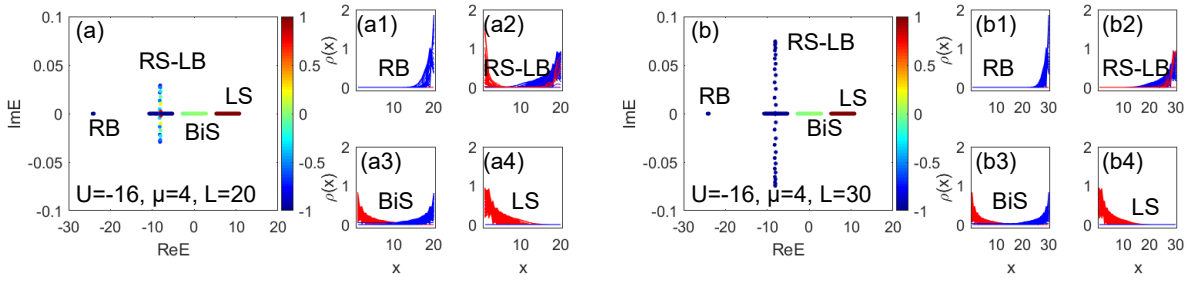

Supplemental Figure 3. The energy spectrum and density distributions versus system size L with $U = -16, \mu = 4$ for $N = 2$. (a) The energy spectrum for $L = 20$. (a1-a4) The densities of the energy clusters ordered by the real energy in (a) indicated by RS, BiS, LS-RB, and LB. (b) the same as (a) but for $L = 30$. In all density plots, the red (blue) curve represents the density on the A (B) sublattice. $J_p = 0.01$ and other parameters are the same as in the main text ($Je^{\alpha} = 1$ and $Je^{-\alpha} = 0.5$).

with $\rho_A = \mathrm{Tr}_B[\rho] = \mathrm{Tr}_B[|\psi\rangle\langle\psi|]$ and

$$S_{\mathrm{left}} = -\mathrm{Tr}\rho_{\mathrm{left}} \ln \rho_{\mathrm{left}} \tag{S11}$$

with $\rho_{\mathrm{left}} = \mathrm{Tr}_{\mathrm{right}}[\rho] = \mathrm{Tr}_{\mathrm{right}}[|\psi\rangle\langle\psi|]$. Here "left" ("right") indicates the left (right) half of lattice, and $|\psi\rangle$ represents the eigenstate with maximum imaginary energy. We find that S_A and S_{left} approximately take the same value across different system sizes. Specifically, they increase and reach a maximum value then decay to zero with the increasing of the system size. The transition from nonzero to zero entropy corresponds to that the bipolar-like state occupying both chains evolves to a left-localized state mainly occupying chain A. This transition is further verified by the density ratio on chain A (ρ_A/N) and on the left half of the system (ρ_{left}/N), which are also shown in Supplemental Figure 5.

Supplemental Note 5. THE THIRD ORDER OF CSE FOR $N = 3$

In our study, the emergence of CSE is mainly characterized by the real-complex transition of eigenenergies, which occurs at different values of J_p depending on the orders of CSE, as shown in Fig. 5 of the main text. In particular, the 3rd-order CSE occurs at a relatively large interchain coupling comparable with other hopping parameters ($J_p = 0.8$),

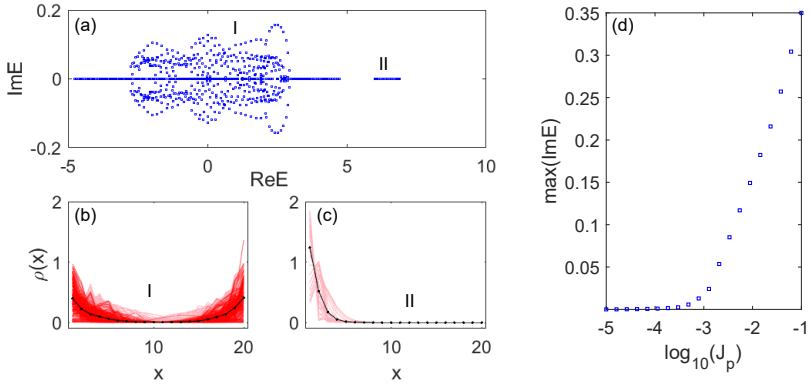

Supplemental Figure 4. The energy spectrum and density distributions of $L = 20$ with $U = 4, \mu = 1, J_p = 0.01$ for $N = 2$. (a) The energy spectrum for $L = 20$. Cluster I consists all the three scattering clusters and one bound cluster in Fig. 3(a) in the main text. (b-c) The densities of the energy clusters ordered by the real energy in (a). The pink lines are density of each states and the black dot for the average density of each cluster. (d) The maximum imaginary energy for the mixed energy cluster I versus coupling strength J_p. Other parameters are the same as in the main text ($Je^{\alpha} = 1$ and $Je^{-\alpha} = 0.5$).

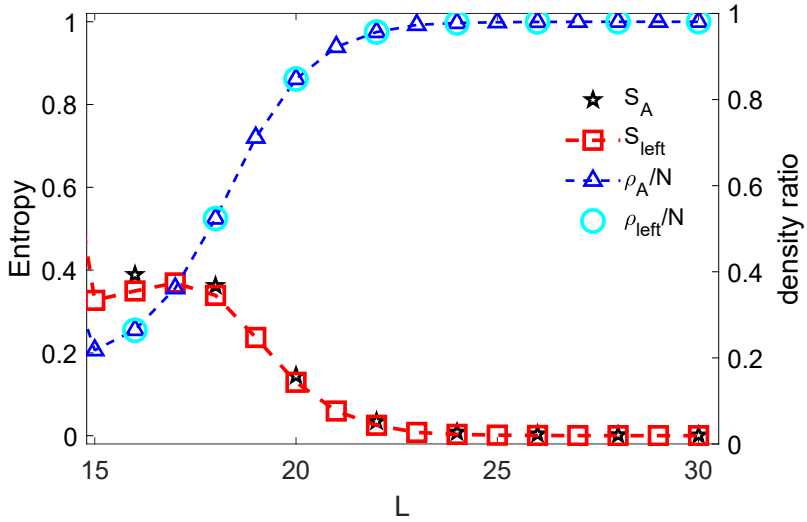

Supplemental Figure 5. Entropies and density ratios of the maximum state for the joint LS-RB cluster ([see Supplemental Figure 2(a) and (b), and Fig. 3(b) in the main text], defined between different chains or different halves of the system. S_A (black star) is the entropy for the A chain by tracing out the B chain. S_{left} (red square) is the entropy for the left-half of the lattice. ρ_A/N (blue triangular) is the ratio of the particle density on chain A to the total density. ρ_{left}/N (blue triangular) is the ratio of the particle density on the left-half of the lattice to the total particle number N. the A chain density to the total density. ρ_{left}/N (cyan circle) is the ratio of the left-half lattice to N. Other parameters are the same as in the main text ($Je^{\alpha} = 1$ and $Je^{-\alpha} = 0.5$).

which seems to diverge from the critical regime for the single-particle CSE with a vanishing J_p. However, we note that in CSEs, the treshold of J_p to induce the transition is expected to decrease as the system size increases. In Supplemental Figure 6, we demonstrate the maximum imaginary energy of the states with 3rd-order CSE for several different system sizes L. It is seen that eigenenergies acuqire imaginary values at weaker J_p for larger L, verifying the higher order criticality of the concerned states.

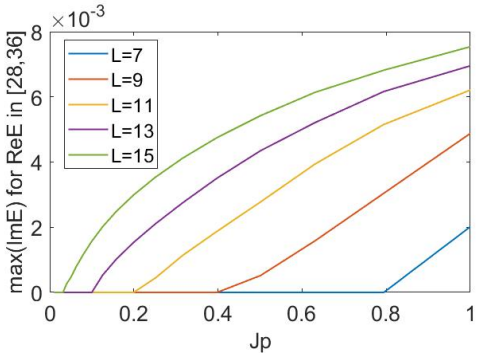

Supplemental Figure 6. Maximum imaginary energy of the states with 3rd-order CSE for $N = 3$ at $U = 16$ and $\mu = 5.333$ [indicated in Fig. 5(d) of the main text]. The treshold of J_p to induce nonzero imaginary energies is found to deacrease with increasing system size. Other parameters are the same as in the main text ($Je^{\alpha} = 1$ and $Je^{-\alpha} = 0.5$).

Supplemental Note 6. THE CRITICAL SKIN EFFECT FOR FERMIONS

In the main text we have provided examples and discussion of many-body CSE for bosons. In this section, we present results for many-body CSE with fermions. The fermoinic analog of our model can be written as

$$\begin{aligned}\hat{H} = &-\sum_{j=1}^{L-1}\sum_{\sigma=A,B} J\left(e^{\alpha_\sigma}\hat{c}^\dagger_{j,\sigma}\hat{c}_{j+1,\sigma} + e^{-\alpha_\sigma}\hat{c}^\dagger_{j+1,\sigma}\hat{c}_{j,\sigma}\right)\\ &+ J_p\sum_{j=1}^{L}\left(\hat{c}^\dagger_{j,A}\hat{c}_{j,B} + \hat{c}^\dagger_{j,B}\hat{c}_{j,A}\right)\\ &+ U_{NN}\sum_{j=1}^{L-1}\sum_{\sigma=A,B}\hat{n}_{j,\sigma}\hat{n}_{j+1,\sigma}\\ &+ \mu\sum_{j=1}^{L}\left(\hat{n}_{j,A} - \hat{n}_{j,B}\right),\end{aligned} \tag{S12}$$

where $\alpha_A = \alpha, \quad \alpha_B = -\alpha$. The onsite-Hubbard interaction for bosons is replaced by a nearest-neighbor interaction U_{NN} for fermions, while other parameters remain the same. The main finding of our paper suggests that CSE can emerge when two parts are spatially separated but energetically connected (facilitating tunneling). Here, we present results for two fermions in Supplemental Figure 7. In the fermionic system, the bound state consists of two nearest-neighbor fermions. The energy spectrum becomes complex with increasing system size, indicating the emergence of many-body CSE.

[S1] Y. Qin and L. Li, Phys. Rev. Lett. **132**, 096501 (2024).
[S2] B. H. Kim, J.-H. Han, and M. J. Park, Communications Physics **7**, 73 (2024).
[S3] T. Orito and K.-I. Imura, Phys. Rev. B **105**, 024303 (2022).

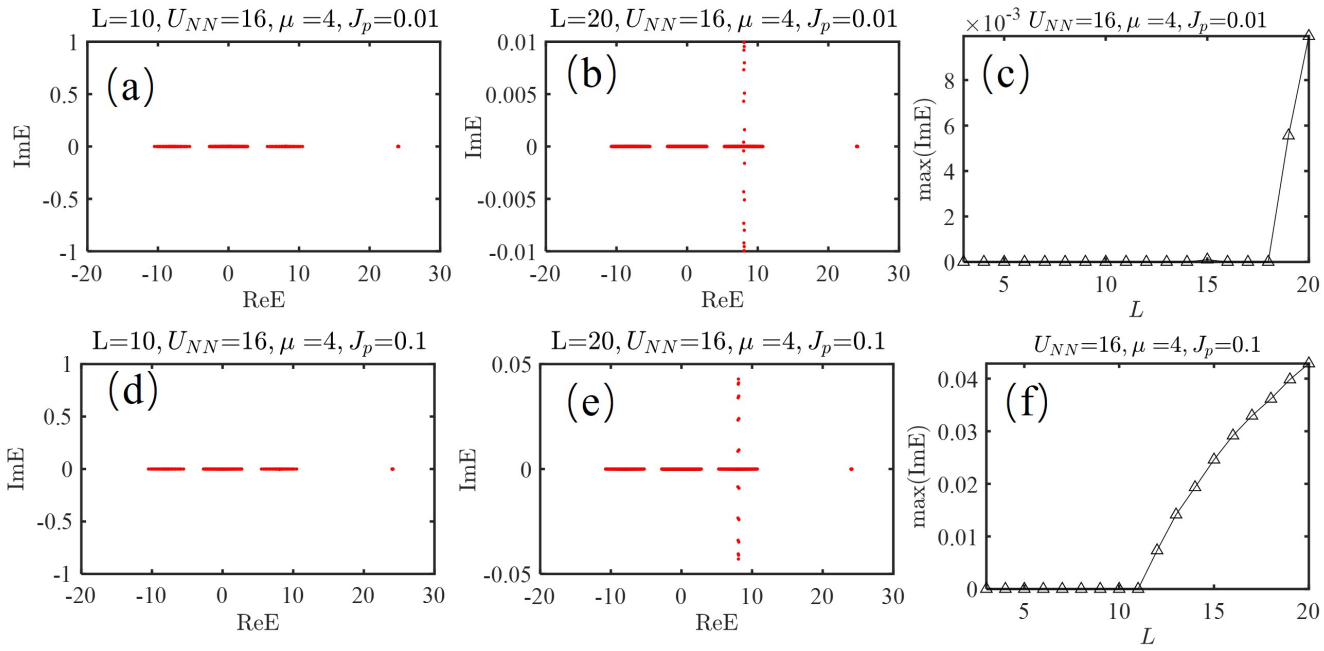

Supplemental Figure 7. The many-body mixed CSE for fermions. The energy spectrum for (a) $L = 10$ and (b) $L = 20$, with $U_{NN} = 16$, $\mu = 4$, and $J_p = 0.01$. (c) The maximum imaginary part of the energy versus L, where a sharp transition indicates the emergence of the critical skin effect. (d–f) Same as (a–c), but with a larger coupling strength $J_p = 0.1$. As shown in (f), the real-complex transition of eigenenergies occurs at a smaller L for stronger J_p. Other parameters are the same as in the main text ($Je^{\alpha} = 1$ and $Je^{-\alpha} = 0.5$).